Simulation of STEM-HAADF Image Contrast of Ruddlesden-Popper Faulted $LaNiO_3$ Thin Films

C. Coll[1], L. López-Conesa[1], J. M. Rebled[1], C. Magén[2,3], F. Sánchez[4], J. Fontcuberta[4], S. Estradé[1], F. Peiró[1*]

1.Laboratory of Electron NanoScopies, LENS-MIND-IN2UB, Dept. Electrónica, Universitat de Barcelona, Marti i Franqués 1, 08028 Barcelona, Spain

2.Laboratorio de Microscopías Avanzadas (LMA), Instituto de Nanociencia de Aragón (INA), Departamento de Física de la 3. Materia Condensada, Universidad de Zaragoza, 50018 Zaragoza, Spain

4.Fundación ARAID, 50018 Zaragoza, Spain

5.Institut de Ciència de Materials de Barcelona (ICMAB-CSIC), Campus UAB, 08193 Bellaterra, Barcelona, Spain

Abstract: $LaNiO_3$ (LNO) thin films are widely used as electrode materials. Yet, their properties greatly depend on such parameters as strain state and defect density. In this work we present a detailed structural characterization of epitaxial LNO thin films grown on $LaAlO_3$(001). Based on scanning transmission electron microscope - high-angle annular dark-field imaging (STEM-HAADF) contrast analysis and image simulations, Ruddlesden-Popper faulted configurations, with 1/2a<111> relative displacement of defect free perovskite blocks, are atomically modeled and simulated to disentangle the variation of Z-contrast in the experimental images.

Introduction:

$LaNiO_3$ (LNO) is of high interest because of its exceptional transport properties, with a resistivity around 100 μΩ·cm at room temperature, and the potential tuning of electrical and magnetic interactions through appropriated strain engineering. Epitaxial strain can induce phase transitions, tuning the interactions between charge, spins and phonons[1]. A precise control of the stoichiometry, structural phases, lattice distortions and the presence/absence of dislocations/defects is critical to use LNO as electrode in epitaxial oxide heterostructures [2–7].

Threading dislocations (TD) and stacking faults (SF) are frequently present in perovskite epitaxial thin films. The usual 1/2a<111> or 1/2a<110> SF translational vectors can be identified through the projection of the corresponding lattice displacements along <100>. The first case is often referred to as Ruddlesden Popper (RP) faults and the relative displacement of the two perfect defect free perovskite ABO_3 blocks a distance of half- unit cell along the [111] direction gives rise to a 1/2a<110> translation in <100> projections, with a typical zig-zag arrangement of the A cations and a BO_2 plane lost at the defect boundary.

The earlier observations of RP faults were based on diffraction results [8,9], but they have also been imaged more recently using advanced microscopy tools, especially by atomic resolution on scanning transmission electron microscope - high-angle annular dark-field imaging (STEM-HAADF) because of its chemical sensitivity at high and low spatial resolution through Z-contrast [10]. Lately, based on HAADF contrast and Electron Energy Loss Spectroscopy(EELS) measurements, some atomistic models have been proposed to describe the geometry and origin of the RP faults in different perovskite materials such as $LaNiO_3$-$LaAlO_3$ [11,12], $La_2SrMn_3O_{10}$ [13], $La_{0.5}Sr_{n+1-0.5}Ti_nO_{3n-1}$ [14], $BaSnO_3$[15], $(Sr,Ca)TiO_3$ [16,17] and (Bi,Ta)CuO [18]. This type of defects critically affects the electronic properties of these compounds, as they can trigger secondary effects as cation diffusion through the defects path or even induce exciting new properties at the interfaces [19].

The presence of RP faults is of special relevance in the so-called Ruddlesden Popper compounds of the type $(A1_xA2_{1-x})_{n+1}B_nO_{3n+1}$. In these RP-n series, the trivalent (A1) and divalent (A2) cations may occupy distinct sites in pure perovskite or rock-salt planes enabling chemical ordering as a function of the A1/A2 ratio in the compound [20]. As an example, STEM-HAADF imaging and contrast measurements of dynamic EELS mapping simulations have been used to analyze this chemical ordering on $La_{2-2x}Sr_{1+2x}Mn_2O_7$ with the aim to discuss the possible concom-

itant charge ordering effects inducing colossal magnetoresistance properties in this compound.

In the present work the attention is focused on the interpretation of changes of contrast in experimental STEM-HAADF images of epitaxial LNO thin films grown on (001) oriented $LaAlO_3$ (LAO) substrates. Different defect-free/RP-faulted combinations in the LNO perovskite crystal are systematically addressed through appropriated atomistic modeling and corresponding STEM-HAADF image simulations in comparison with the experimental results. We illustrate that the expected Z-contrast between A and B sites gradually vanishes or even disappears as a consequence of superposition of pure perovskite-RP displaced blocks, without the need of considering additional structural disorder or cation mixing in the crystals.

Experimental details:

LNO thin films, 35 nm thick, were grown on LAO(001) by pulsed laser deposition (PLD) using a KrF excimer laser (λ=248 nm) with a fluence of around 1.5 J cm^{-2} and a repetition rate of 5 Hz. Deposition was performed at an oxygen pressure of 0.15 mbar and keeping the substrate at a temperature of 700°C.

Samples were prepared for Transmission Electron Microscopy (TEM) observation either by the Focused Ion Beam (FIB) lift-out technique in an FEI Strata 235 Dual Beam or by mechanical polishing and subsequent low angle Ar^+ ion milling getting a thickness of 50 nm of the observable region. They were observed in a JEOL 2010F TEM at 200 keV, for high resolution imaging, and also using an aberration probe corrected FEI Titan TEM at 300 keV for atomically resolved STEM-HAADF.

The HAADF images were simulated by the multislice Cowley and Moddie method [21], which solves the problem of propagation of a quantum mechanical wave through a crystal potential. The sample is divided in slices and the transmitted wave is computed at every slice. From an optics viewpoint the propagator function can be associated with Fresnel diffraction.

The software package used to perform the HAADF simulations was TEMsim package developed by E. Kirkland [22]. The structure files used as a simulation input were generated using the Rhodius package of University of Cadiz [23,24].This software allows obtaining supercells from the combination of different periodical building blocks, so that complex structures, such as dislocations or interfaces, can be modeled.

The experimental parameters used as an input for image simulation were a voltage of the incident beam of 300 keV and a spherical aberration coefficient of 1 μm. The condenser aperture was set at 24 mrad. The defocus, spherical aberration coefficient and the number of pixels were set to get atomic resolution simulated images, similar to the experimental ones.

The angular range of the HAADF detector was set between 55mrad and 300 mrad, according to the experimental setup. The simulations were repeated several times in order to find the right defocus. Defocus parameter was adjusted to obtain the best fit between simulations and experimental images.

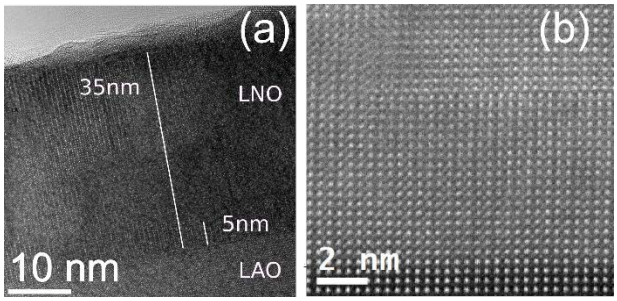

Figure 1. (a) HRTEM image of LNO thin films. (b) HAADF STEM image of LNO thin film defects.

Results and discussion:

The LNO films grow epitaxially on the LAO substrate even if the lattice mismatch between LNO and LAO is of 1% (the lattice parameter of LAO is 3.79 Å and for LNO it is of 3.83 Å). LNO shows [010]LNO(001)//[010]LAO(001) cube-on-cube epitaxial relationship, and atomic-sharp interface with the substrate (Fig. 1(a)).

The first 5 nm LNO grows fully coherent to the substrate under a compressive stress. However, 5 nm far from the interface, HAADF image highlights the presence of defective regions, probably acting as a stress-relieving mechanism (Figure 1(b)), this is explained in more detail in [25]. One example of the most frequent defect is shown in

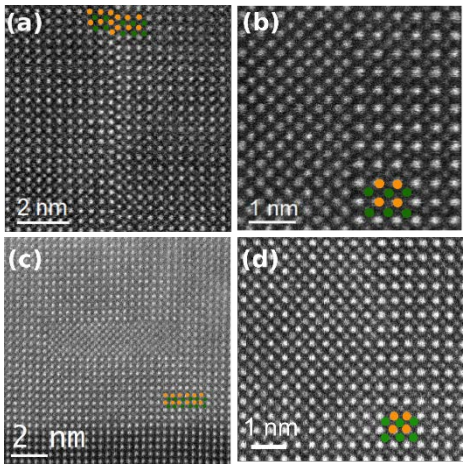

Fig. 2 Experimental HAADF images of the LNO thin films where orange balls correspond to lanthanum atoms and green ones to nickel. (a) LNO film region containing a 2D planar defect with the characteristic zig-zag of the La atoms. (b) LNO film region showing the Z-contrast of a perovskite structure on [100] zone axis in the right side; in the left side the contrast is lost. (c) LNO film region showing a central region with no contrast (d) LNO film region showing a gradual loss of perovskite Z contrast when moving from right to

Figure 2a, where two defect free perovskite crystal regions, with cationic positions of La (orange) and Ni (green), easily recognized from the different intensity according to the distinct atomic number (due to Z contrast, La columns are brighter that Ni columns), appear displaced from each other. This is further observed through EELS mapping of the region (Fig 3). We can see a relative shift of A and B sites of 1/2a<110>, and the introduction of a rock salt layer (AO) (loss of Ni plane) at the defect line. This configuration can be identified as a Ruddlesden Popper fault with translational vector 1/2a<111>, giving rise to a 1/2a<110> displacement of lanthanum atoms when observed along the [001] zone axis.

Besides these vertical lineal RP faults, some other defects are found in the LNO layer. In Fig. 2b a defect line similar to that of a RP fault is observed, this time aligned horizontally along the [010] direction. However, in this case the expected Z-contrast is not preserved at the left side of the image, where we cannot differentiate the occupancy of A/B sites of the perovskite by La or Ni, due to the homogeneity of the contrast in all columns. Regions with a similar loss of contrast are also observed, but with well-defined boundaries delimiting rectangular shapes, as illustrated in Figure 2c. A rectangular block of homogenous intensity for A/B sites is surrounded by regions with the usual perovskite Z-contrast. A more complex case is presented in Fig. 2d. As we move from right to left, a gradual loss of contrast is observed; on the left side the contrast is completely lost and A/B positions are impossible to tell apart.

STEM-HAADF simulations were performed in order to understand the intimate atomic structural configuration giving rise to the observed Z-contrast, disregarding any chemical intermixing or phase segregation that could also induce such a contrast fading [26].

The first step was to verify the identification of the Ruddlesden Popper fault observed in figure 2a. A RP fault basically implies the displacement of a half of the unit cell on the [111] direction. The missing NiO_2 plane produces the zig-zag arrangement of the lanthanum atoms as described by Detemple *et al*.

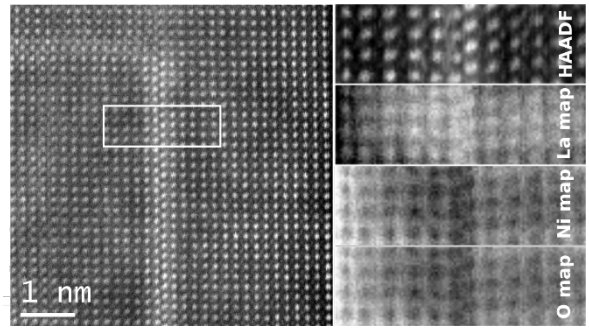

Fig. 3 HAADF image and ~~its~~ EELS composition maps show~~s~~ that ~~at the~~a NiO_2 plane has been suppressed and a zig-zag ~~arengament~~ arrangementt of the La atoms ~~have appeare~~is apparent as a consequence~~d~~.

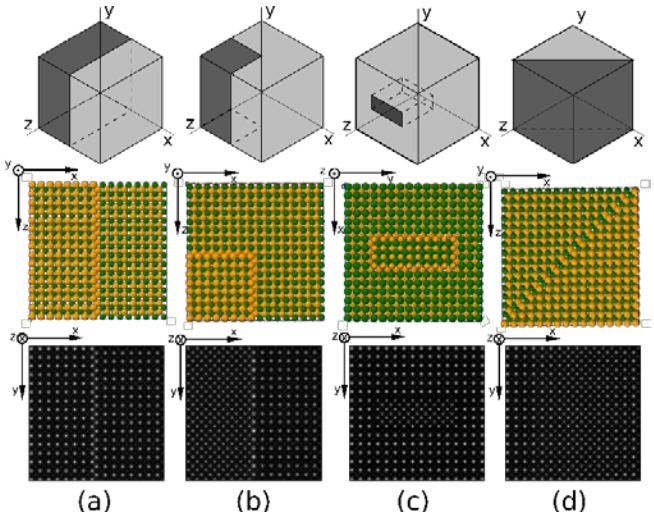

Fig. 4 (1st row) 3d models of the supercells configurations, where the darkest regions correspond to the blocks displaced. (2nd row) Atomistic models of RP of different configurations proposed to explain the aforementioned defects found in LNO thin films, where green balls correspond to nickel atoms and orange ones to lanthanum. In the HAADF simulations, the electron beam was considered parallel to the z axis. (3rd row) HAADF simulation results. A good agreement with the experimental images in figure 2 is observed, which validates the proposed models.

Therefore, an atomistic model of 60×60×60 Å size was then built by adding two perfect perovskite crystals with a relative displacement of a half of the unit cell along the [111] direction, as the 3D model of figure 4a shows. The configuration of such a supercell is schematically shown in figure 4a, where green balls correspond to nickel atoms and orange ones to lanthanum atoms, considering that the fault boundary is parallel to the electron beam and perpendicular to the cross-section view. From this model, a HAADF image simulation was obtained.

Once the contrast in Figure 2a was properly disentangled as explained by the existence of a RP fault between two blocks of perfect perovskite structure, the elucidation of the rest of the casuistic was addressed through the atomistic modeling of more complex configurations obtained also by combining displaced defect-free perovskite blocks.

Considering the case of Figure 2b, we assumed that the homogeneity of Z-contrast could be due to an average of the atomic numbers of La and Ni because of the mixed occupancy in A and B sites when viewed in a [001] projection. A supercell was built with a block of 30x60x30 Å displaced 1/2a<111> with respect to the rest of the defect free region, leading to an overlapping of the RP displaced perovskite blocks in the direction of the electron beam (z direction in the schemes) just in one half of the model as shown in Figure 4b (top and middle). The results of the simulation are shown in Figure 4b (bottom). The correspondence with the experimental image (Figure 2b) confirms the modeled configuration.

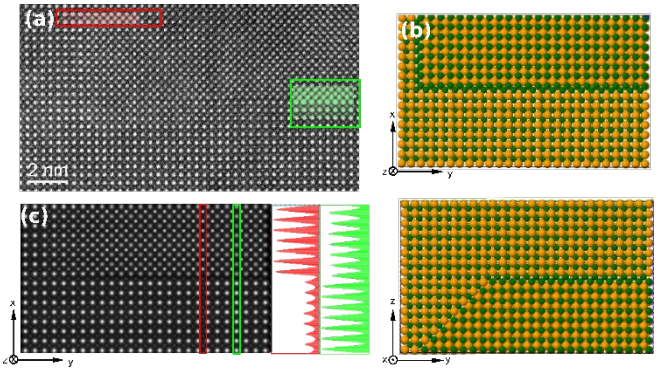

Fig. 5 (a) Experimental HAADF image of a $LaNiO_3$ thin film. Simulation results are superimposed. (b) Proposed atomic model for the HAADF contrast in (a), as viewed along the y (up) and the z (down) axes (c). Simulated HAADF image from the model in (b). Compare it with the experimental image in (a). On the left-hand side, the intensity profiles corresponding to the highlighted regions are given.

Similarly, taking into account the contrast in Figure. 2c, we modeled an orthorhombic block of 30 Å in thickness and a base of 35×12 Å displaced from the surrounding matrix, according to the model in figure 4c. The results of the simulation effectively show the homogeneity of contrast in the region of the overlapping perovskite blocks, validating the proposed model.

Finally, as far as the gradual variation of contrast is concerned, a model containing two perovskite blocks with the RP boundary oriented at 45 degrees with respect to the electron beam was considered, along a (011) plane. This situation is equivalent to the overlapping of two displaced perovskite blocks with opposite thickness gradients as schematically shown in Figure 4d (top and middle). Figure 4d (bottom) shows the simulated HAADF image, with the expected contrast.

The good agreement between HAADF simulations and experimental images validates the proposed models for the defects found in these regions: namely, the occurrence of RP faults in different geometries.

The contrast observed in wider regions can be also accounted for an adequate combination of perovskite RP displaced blocks.

Figure 5a shows an experimental image where the two highlighted regions can be identified with some of the previous modeled cases. In the lower left side (highlighted in green) there is a region with and without A/B sites contrast, which corresponds to the configuration described by the model in Figure 4b. In the upper part of the image, a gradual loss of contrast can be observed (highlighted in red) that corresponds to the previous model in Figure 4d. Thus, a final atomic model of 60×100×60 Å was built combining both models, as shown in two projections in figure 4b. The result of the simulation using this supercell model fully recovers the HAADF contrast observed in the experimental image (Fig. 5c).

Z-contrast intensity profiles along two atomic columns highlight the averaging of contrast in the upper section of the simulated image in Figure 4c, since both profiles present similar intensity maxima. Conversely, on the bottom part, one profile presents a lower intensity when compared to the other, as expected for LaO and NiO_2 columns, respectively. From the modelitzation of this gradual loss of perovskite characteristic contrast we have checked that the vanishing occurs once the overlapping is between a 37.5% and 62,5% of nickel/lanthanum atoms. Thus, the samples have an overlapping of layers between 20 and 30 nm inthickness.

HAADF image simulations have thus allowed to explain an interesting lack of atomic contrast in LNO HAADF images as a purely geometric effect stemming from the presence of RP faults on the film, as opposed to segregation or interdiffusion phenomena, in very good agreement with the model proposed by Detemple *et al*. This highlights the importance of a careful microstructural characterization to unveil the information contained in HAADF images and the convenience of simulations to validate the suggested atomic models.

Conclusions:

LNO thin films have been grown on a LAO substrate with good crystalline quality, good cube-on-cube growth fulfilling the [001]LNO(010)//[001]LAO(010) epitaxial relationship, and atomically sharp interfaces. The presence of RP faults in different combinations with defect free regions have been described.

HAADF simulations based on multislice Cowley and Moodie method have been used as a tool to identify these defects as RP faults. Atomistic supercell models have been built by the combination of defect free perovskite blocks displaced 1/2a<111> from each other. A loss of image contrast for atomic columns corresponding to A and B sites has been observed, which can be explained in terms of the overlapping of La and Ni columns in RP displaced perovskite blocks. More complex gradual variation of Z-contrast levels has also been observed and has been found to correspond to a variation of the thickness of the overlapped perovskite blocks.

Modeling of large supercells with appropriated combination of RP displaced perovskite blocks has enabled the simulation of wide regions of the LNO thin films, and, finally, a complete understanding of the experimental HAADF contrast.

Corresponding Author

*francesca.peiro@ub.edu

ACKNOWLEDGMENT

Financial support by the Spanish Government (Projects MAT2013-41506-P and MAT2014-56063-C2-1-R) and Generalitat de Catalunya (2014-SGR-734 and 2014-SGR-672) is acknowledged. ICMAB-CSIC authors acknowledge financial support from the Spanish Ministry of Economy and Competi-

tiveness, through the “Severo Ochoa” Programme for Centres of Excellence in R&D (SEV- 2015-0496).

References:

(1) Weber, M. C.; Guennou, M.; Dix, N.; Pesquera, D.; Sánchez, F.; Herranz, G.; Fontcuberta, J.; López-Conesa, L.; Estradé, S.; Peiró, F.; et al. Multiple Strain-Induced Phase Transitions in LaNi O3 Thin Films. *Phys. Rev. B - Condens. Matter Mater. Phys.* **2016**, *94* (1).

(2) Miyazaki, H.; Goto, T.; Miwa, Y.; Ohno, T.; Suzuki, H.; Ota, T.; Takahashi, M. Preparation and Evaluation of LaNiO3 Thin Film Electrode with Chemical Solution Deposition. *J. Eur. Ceram. Soc.* **2004**, *24* (6), 1005–1008.

(3) Kharton, V. V.; Yaremchenko, A. A.; Shaula, A. L.; Patrakeev, M. V.; Naumovich, E. N.; Logvinovich, D. I.; Frade, J. R.; Marques, F. M. B. Transport Properties and Stability of Ni-Containing Mixed Conductors with Perovskite- and K2NiF4-Type Structure. *J. Solid State Chem.* **2004**, *177* (1), 26–37.

(4) Hwang, J.; Son, J.; Zhang, J. Y.; Janotti, A.; Walle, C. G. Van De; Stemmer, S. Structural Origins of the Properties of Rare Earth Nickelate Superlattices. *Phys. Rev. B* **2013**, *60101*, 2–5.

(5) Kinyanjui, M. K.; Lu, Y.; Gauquelin, N.; Wu, M.; Frano, A.; Wochner, P.; Reehuis, M.; Christiani, G.; Logvenov, G.; Habermeier, H. U.; et al. Lattice Distortions and Octahedral Rotations in Epitaxially Strained LaNiO3/LaAlO3 Superlattices. *Appl. Phys. Lett.* **2014**, *104* (22), 3–7.

(6) Zhu, M.; Komissinskiy, P.; Radetinac, A.; Vafaee, M.; Wang, Z.; Alff, L. Effect of Composition and Strain on the Electrical Properties of LaNiO3 Thin Films. *Appl. Phys. Lett.* **2013**, *103* (14), 141902.

(7) Scherwitzl, R.; Zubko, P.; Lichtensteiger, C.; Triscone, J. M. Electric-Field Tuning of the Metal-Insulator Transition in Ultrathin Films of LaNiO3. *Appl. Phys. Lett.* **2009**, *95* (22), 10–13.

(8) Ruddlesden, S. N.; Popper, P. The Compound Sr3Ti2O7 and Its Structure. *Acta Crystallogr.* **1958**, *11*, 54–55.

(9) Ruddlesden, S. N.; Popper, P. New Compounds of the K 2 NIF 4 Type. *Acta Crystallogr.* **1957**, *10* (8), 538–539.

(10) Recnik, A.; Möbus, G.; Strum, S. IMAGE-WARP□: A Real-Space Restoration Method for High-Resolution STEM Images Using Quantitative HRTEM Analysis. *Ultramicroscopy* **2005**, *103*, 285–301.

(11) Detemple, E.; Ramasse, Q. M.; Sigle, W.; Cristiani, G.; Habermeier, H. U.; Benckiser, E.; Boris, A. V.; Frano, A.; Wochner, P.; Wu, M.; et al. Polarity-Driven Nickel Oxide Precipitation in LaNiO3-LaAlO 3 Superlattices. *Appl. Phys. Lett.* **2011**, *99* (21).

(12) Detemple, E.; Ramasse, Q. M.; Sigle, W.; Cristiani, G.; Habermeier, H. U.; Keimer, B.; Van Aken, P. A. Ruddlesden-Popper Faults in LaNiO 3/LaAlO 3 Superlattices. *J. Appl. Phys.* **2012**, *112* (1), 1–6.

(13) Palgrave, R. G.; Borisov, P.; Dyer, M. S.; Mcmitchell, S. R. C.; Darling, G. R.; Claridge, J. B.; Batuk, M.; Tan, H.; Tian, H.; Verbeeck, J.; et al. Artificial Construction of the Layered Ruddlesden – Popper Manganite La2Sr2Mn3O10 by Reflection High Energy Electron Diffraction Monitored Pulsed Laser Deposition. *J. Am. Chem. Soc.* **2012**, *134*, 7700–7714.

(14) Tokuda, Y.; Kobayashi, S.; Ohnishi, T.; Mizoguchi, T.; Shibata, N.; Ikuhara, Y.; Yamamoto, T. Growth of Ruddlesden-Popper Type Faults in Sr-Excess SrTiO3 Homoepitaxial Thin Films by Pulsed Laser Deposition. *Appl. Phys. Lett.* **2011**, *99* (17), 5–8.

(15) Wang, W. Y.; Tang, Y. L.; Zhu, Y. L.; Suriyaprakash, J.; Xu, Y. B.; Liu, Y.; Gao, B. Atomic Mapping of Ruddlesden-Popper Faults in Transparent Conducting BaSnO 3 -Based Thin Films. *Sci. Rep.* **2015**, No. August, 1–9.

(16) Fujimoto, M.; Suzuki, T.; Nishi, Y.; Arai, K. Calcium-Ion Selective Site Occupation at Ruddlesden – Popper-Type Faults and the Resultant Dielectric Properties of A-Site-Excess Strontium Calcium Titanate Ceramics. *J. Am. Ceram. Soc.* **1998**, *40*, 33–40.

(17) Wang, Z.; Okude, M.; Saito, M.; Tsukimoto, S.; Ohtomo, A.; Tsukada, M.; Kawasaki, M.; Ikuhara, Y.; Wang, Z. Dimensionality-Driven Insulator-Metal Transition in A-Site Excess Non-Stoichiometric Perovskites. *Nat. Commun.* **2010**, *1* (8), 106–107.

(18) Suzuki, T.; Nishi, Y.; Fujimoto, M. Ruddlesden–Popper Planar Faults and Nanotwins in Heteroepitaxial Nonstoichiometric Barium Titanate Thin Films. *J. Am. Ceram. Soc.* **2000**, *83*, 3185–3195.

(19) Arredondo, M.; Weyland, M.; Hambe, M.; Ramasse, Q. M.; Munroe, P.; Nagarajan, V. Chemistry of Ruddlesden – Popper Planar Faults at a Ferroelectric – Ferromagnet Perovskite Interface Chemistry of Ruddlesden – Popper Planar Faults at a Ferroelectric – Ferromagnet Perovskite Interface. *J. Appl. Phys.* **2011**, *109*, 84101.

(20) Roldan, M. A.; Oxley, M. P.; Li, Q.; Zheng, H.; Gray, K. E.; Mitchell, J. F.; Pennycook, S. J.; Varela, M. Atomic Scale Studies of La / Sr Ordering in Colossal Magnetoresistant La 2 – 2 X Sr 1 + 2 X Mn 2 O 7 Single Crystals. *Microsc. Microanal.* **2014**, *20*, 1791–1797.

(21) Cowley, J. M.; Moodie, A. F. The Scattering of Electrons by Atoms and Crystals. I. A New Theoretical Approach. *Acta Crystallographica*. 1957, pp 609–619.

(22) Kirkland, E. J. *Computation of Transmission Electron Micrographs*; 1998; Vol. 129.

(23) Bernal, S.; Botana, F. J.; Calvino, J. J.; López-Cartes, C.; Pérez-Omil, J. A.; Rodríguez-Izquierdo, J. M. The Interpretation of HREM Images of Supported Metal Catalysts Using Image Simulation□: Profile View Images. *Ultramicroscopy* **1998**, *72*, 135–164.

(24) Pérez-Omil, J. A. Interpretación Sistemática de Imágenes de Microscopía Electrónica de Alta Resolución de Materiales Policristalinos. Estudio de Catalizadores Metálicos Soportados., Univesidad de Cádiz.

(25) López-Conesa, L.; Rebled, J. M.; Pesquera, D.; Dix, N.; Sánchez, F.; Herranz, G.; Fontcuberta, J.; Magén, C.; Casanove, M. J.; Estradé, S.; et al. □Physical Chemistry Chemical Physics, **2017** *in press*.

(26) Smith, C. R.; Lang, A. C.; Shutthanandan, V.; Taheri, M. L.; May, S. J.; Smith, C. R.; Lang, A. C.; Taheri, M. L.; May, S. J. Effects of Cation Stoichiometry on Electronic and Structural Properties of LaNiO3. *J. Vaccum Sci. Technol. A* **2016**, *33* (2015), 41510.